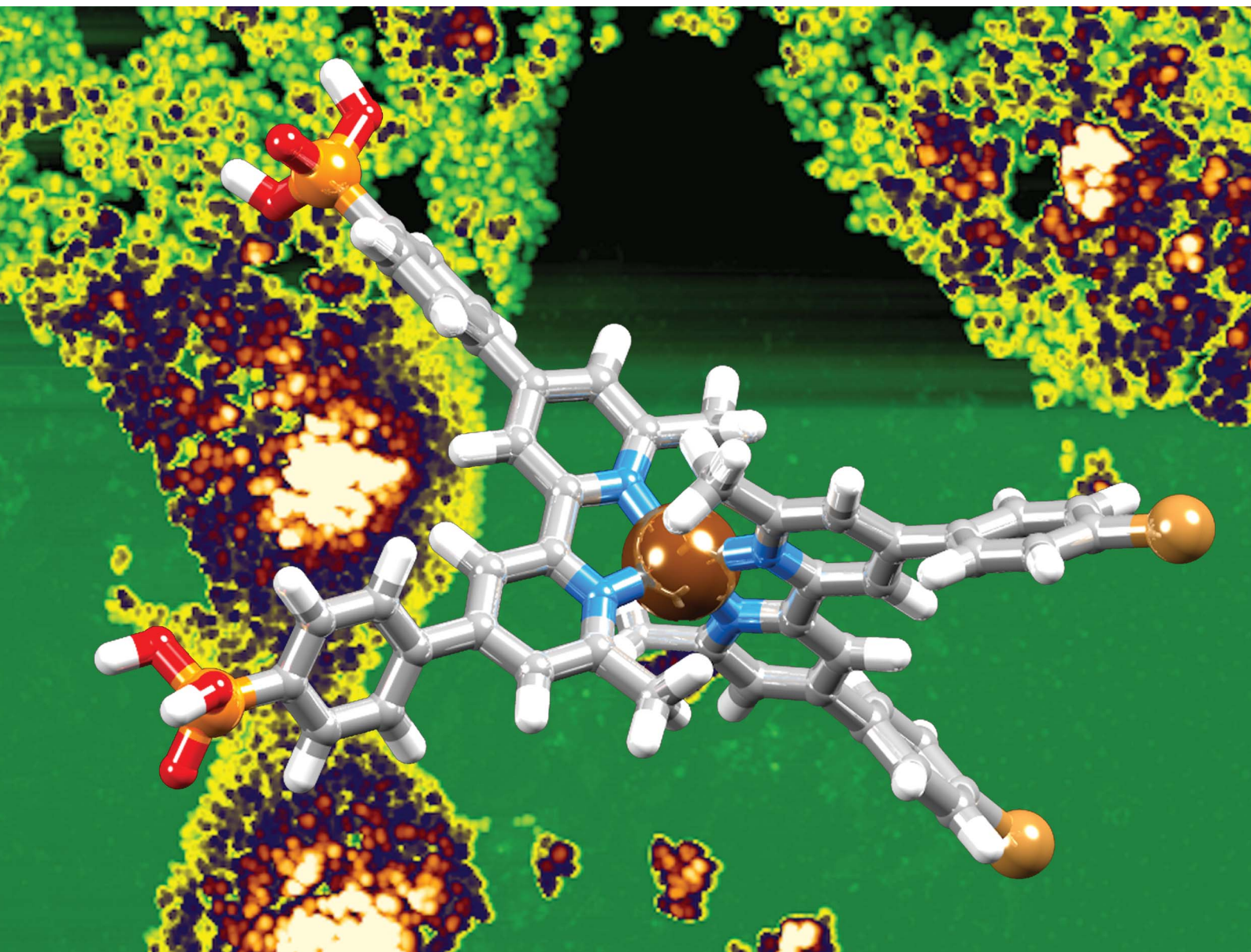


Nanoscale Advances

Volume 2
Number 2
February 2020
Pages 523–914

rsc.li/nanoscale-advances



ISSN 2516-0230


PAPER

Edwin C. Constable *et al.*
The SALSAC approach: comparing the reactivity of
solvent-dispersed nanoparticles with nanoparticulate
surfaces

PAPER

[View Article Online](#)
[View Journal](#) | [View Issue](#)Cite this: *Nanoscale Adv.*, 2020, 2, 679

The SALSAC approach: comparing the reactivity of solvent-dispersed nanoparticles with nanoparticulate surfaces†

Sven A. Freimann,  Davood Zare,  Catherine E. Housecroft 
and Edwin C. Constable *

We demonstrate that the 'surface-as-ligand, surface-as-complex' (SALSAC) approach that we have established for annealed nanoparticulate TiO₂ surfaces can be successfully applied to nanoparticles (NPs) dispersed in solution. Commercial TiO₂ NPs have been activated by initial treatment with aqueous HNO₃ followed by dispersion in water and heating under microwave conditions. We have functionalized the activated NPs with anchoring ligands 1–4; 1–3 contain one or two phosphonic acid anchoring groups and 4 has two carboxylic acid anchors; ligands 1, 2 and 4 contain 6,6'-dimethyl-2,2'-bipyridine (Me₂bpy) metal binding domains and 3 contains a 2,2':6',2''-terpyridine (tpy) unit. Ligand functionalization of the activated NPs has been validated using infrared and ¹H NMR spectroscopies, and thermogravimetric analysis. NPs functionalized with 1, 2 and 4 react with [Cu(MeCN)₄][PF₆] and those with 3 react with FeCl₂·4H₂O; metal binding has been investigated using solid-state absorption spectroscopy and scanning electron microscopy (SEM). Competitive binding of ligands 1–4 to TiO₂ NPs has been investigated and shows preferential binding of phosphonic acid over carboxylic acid anchors. For the phosphonic acids, the binding orders are 3 > 1 > 2 which is rationalized in terms of relative pK_a values (phosphonic acid and [HMe₂bpy]⁺ or [Htpy]⁺) and the number of anchoring groups in the ligands. Ligand exchange between ligand-functionalized NPs and homoleptic metal complexes gives NPs functionalized with heteroleptic copper(i) or iron(ii) complexes.

Received 8th August 2019
Accepted 12th December 2019

DOI: 10.1039/c9na00488b

rsc.li/nanoscale-advances

Introduction

Numerous methodologies have been developed for the synthesis of hierarchical structures^{1–4} at interfaces, including self-assembled monolayers,^{5–7} self-organization and self-assembly^{8,9} through van der Waals forces^{10–12} supramolecular chemistry,¹³ templating,¹⁴ sol–gel deposition techniques,¹⁵ pyrolysis⁴ and dye-stamping.¹⁶ In most cases the methods are either highly specific to the target structure, are dependent upon the preparation of complex soluble or volatile covalent structures or have significant elements of serendipity in the outcome.¹⁷

In the context of our research into dye-sensitized solar cells (DSCs), we developed a methodology^{18–20} which we have termed

'surfaces-as-ligands, surfaces-as-complexes' (SALSAC). This extends 'simple' self-assembly and self-organization at surfaces to the stepwise and hierarchical building up of new pre-defined and easily tailored architectures. Our inspiration and motivation lie in an appreciation of the exquisite complexity of biological systems and at the same time a desire to utilize self-assembly and self-organization strategies to achieve similar levels of complexity in synthetic systems. An added value of this approach is that the increasing complexity of the architectures can lead to emergent properties²¹ not found in the individual components. The concept of this paper relates to the transferability of modification reactions between extended surfaces and nanoparticulate materials.

Although we developed the SALSAC approach for the assembly of heteroleptic copper(i) dyes on the surface of semiconductor nanostructured surfaces for use in DSCs,²⁰ it is clear that the experimentally simple approach of sequentially reacting a surface with components leading to a hierarchical assembly has wider applications. In its mature form, SALSAC has been developed into a powerful atom-efficient methodology allowing the preparation of multiply and specifically functionalized surfaces through step-wise assembly of structures incorporating anchoring ligands, metal ions and ancillary ligands.²⁰ The SALSAC approach is illustrated in Fig. 1: a nanoparticulate

Department of Chemistry, University of Basel, BPR 1096, Mattenstrasse 24a, CH-4058 Basel, Switzerland. E-mail: edwin.constable@unibas.ch

† Electronic supplementary information (ESI) available: Instrument details; Fig. S1–S6: mass spectrum and NMR spectra of 2; Fig. S7: DOSY fits; Fig. S8 and S9: IR spectra of NPs functionalized with 1 and 3; Fig. S10: TGA curve of 1; Fig. S11–S13 and S15: NMR spectra of competition experiments; Fig. S14: photographs of activated TiO₂ NPs functionalized 2 and 4; Fig. S16–S21: mass spectrum and NMR and IR spectra of 7; Fig. S22–S29: NMR and IR spectra of [Cu(6)₂][PF₆] and [Cu(7)₂][PF₆]; Fig. S30: absorption spectrum of NPs functionalized with 3 after treatment with [Fe(8)₂][PF₆]₂. See DOI: 10.1039/c9na00488b

surface is modified with a compound (L_{anchor}) which combines an anchoring group specific to the surface (e.g. carboxylic acid, carboxylate, phosphonic acid or phosphonate for a metal oxide) and a metal-binding domain such as 2,2'-bipyridine (bpy) or 2,2':6',2''-terpyridine (tpy). Subsequent reaction with a metal ion (e.g. copper(i) in the case of DSC applications²⁰) and concurrent or consecutive reaction with ancillary ligands ($L_{\text{ancillary}}$) gives a surface functionalized with a heteroleptic metal complex containing both L_{anchor} and $L_{\text{ancillary}}$ ligands. An alternative strategy is to introduce metal ion and $L_{\text{ancillary}}$ by ligand exchange from a homoleptic complex.

Although we have focused on the addition of a single type of ancillary ligand in optimizing DSCs, we have also demonstrated that surfaces can be modified by sequential addition of two different ancillary ligands.²² Further development of this approach has the potential to introduce secondary surface sites which act purely to spatially separate the primary surface sites. In DSC applications, this translates to the introduction of co-adsorbants which can also bind to the metal oxide surface, typically through carboxylic acid or carboxylate, to inhibit molecular-dye aggregation.²³ Spatial separation may also be important in preventing metal-binding domains of surface-attached anchoring ligands from binding the same metal ion, generating surface-bound homoleptic complexes rather than the desired heteroleptic species.²⁴

Although numerous studies have described the attachment of anchor-functionalized complexes to surfaces, few studies relate to initial ligand functionalization of a surface through an anchor.²⁵ While ligand functionalized surfaces have been subsequently metallated,^{26,27} to the best of our knowledge, there has been no systematic investigation of the SALSAC methodology and combined use to introduce functionality through the ancillary ligand other than our own work in the context of copper(i) DSCs. We now explore how the principles established for annealed nanoparticulate TiO_2 surfaces (i.e. working electrodes in DSCs) can be extended to nanoparticles (NPs) of the same material dispersed in fluid phase. The fabrication and applications of functionalized metal oxide NPs is well

established,²⁸ but hierarchical assembly strategies are less well explored. It should be noted that when an anchoring ligand with an acidic functionality such as $-\text{CO}_2\text{H}$ or $-\text{PO}_3\text{H}_2$ is introduced, the protonation state and binding mode of the ligand is typically not well-defined, although the properties of the assembly are critically dependent on the protonation state.^{29–31} The functionalization of metal chalcogenide nanoparticles with carboxylic and phosphoric acids has attracted much recent attention and a few reports of selectivity and exchange of surface-bound ligands have been published.^{32–41}

Experimental

General

Details of instrumentation are given in the ESI.†

The complex $[\text{Cu}(\text{MeCN})_4][\text{PF}_6]$ was prepared by the method of Kubas.⁴² 4-(4-Bromophenyl)-6,6'-dimethyl-2,2'-bipyridine,¹⁸ **1**,⁴⁴ **3**,³⁰ **4**,⁴³ **5**,⁴⁴ **6**,⁴⁵ **8**,⁴⁶ $[\text{Fe}(\text{8})_2][\text{PF}_6]_2$,⁴⁷ and $[\text{Cu}(\text{5})_2][\text{PF}_6]_4$ ⁴⁴ were prepared according to literature and their spectroscopic data matched those previously reported.

TiO_2 nanoparticles (AEROXIDE TiO_2 P25) were purchased from Evonik Industries. The spherical NPs have an average radius of 10.5 nm,⁴⁸ leading to a surface area-to-volume ratio of 28%. In the Experimental section, the number of equivalents of NPs are defined as $0.28 \times$ the total number of TiO_2 formula equivalents in the mass given, i.e. the effective surface concentration of TiO_2 .

Compound 2a

Solid 4-(4-bromophenyl)-6,6'-dimethyl-2,2'-bipyridine (340 mg, 1.00 mmol, 1 eq.), Cs_2CO_3 (1.629 g, 5 mmol, 5 eq.) and $[\text{Pd}(\text{PPh}_3)_4]$ (57.8 mg, 0.05 mmol, 0.05 eq.) were placed in a 20 mL microwave vial under N_2 . Diethyl phosphonate (552 mg, 511 μL , 4 mmol, 4 eq.) and 15 mL dry THF were added. The mixture was degassed by bubbling N_2 for 5–10 min and then the vial was capped. The reaction mixture was heated in the microwave reactor for 5 h at 130 °C and then cooled to room temperature, filtered through Celite and evaporated to dryness. The resulting yellow oil was dissolved in MeCN and the product isolated as pale-yellow crystals which were collected by filtration, washed with cold Et_2O and dried under vacuum (200 mg). The crude product was used in the next step without further purification (see text).

Compound 7

5 (582 mg, 1.18 mmol, 1.0 eq.), Cs_2CO_3 (2.31 g, 7.08 mmol, 6.0 eq.) and $[\text{Pd}(\text{PPh}_3)_4]$ (136 mg, 0.118 mmol, 10 mol%) were added to a microwave vial under N_2 . 3,5-Dimethyl-4-(4,4,5,5-tetramethyl-1,3,2-dioxaborolan-2-yl)isoxazole (1.05 g, 4.72 mmol, 4.0 eq.) and anhydrous toluene (20 mL) were added to another vial and N_2 was bubbled through the solution for 15 min. The contents of the two vials were combined into one microwave vial and N_2 was bubbled through the mixture for 10 min. The vial was sealed and the reaction mixture was heated to 110 °C for 4 h in a microwave reactor, after which time it was allowed to cool to room temperature. Then H_2O (40 mL) was

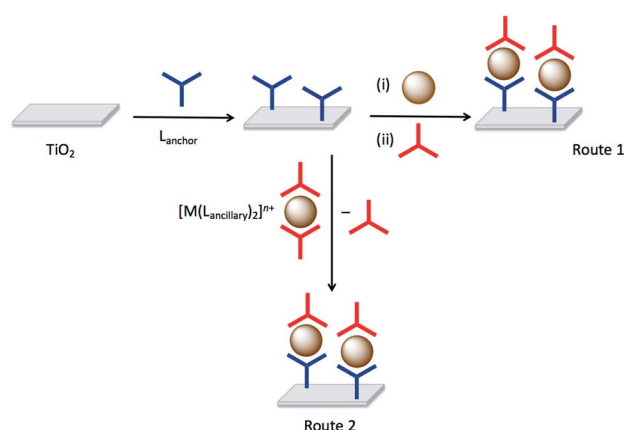


Fig. 1 Surface modification (e.g. nanoparticulate TiO_2) with a single anchor, single metal ion and an ancillary ligand (route 1), or with a single anchor followed by ligand exchange using a homoleptic metal complex (route 2).



added and the reaction mixture was extracted with CH_2Cl_2 (3×50 mL) and dried over anhydrous MgSO_4 . The solvent was removed under reduced pressure to yield an off-white solid. The residue was dissolved in hot CHCl_3 (1 mL), and the product was precipitated by addition of EtOH (10 mL). The precipitate was washed with EtOH (50 mL) and acetone (50 mL) to yield **7** as a beige solid (205 mg, 1.18 mmol, 33%). ^1H NMR (500 MHz, CDCl_3) δ /ppm: 8.55 (d, $J = 1.6$, 2H, H^{A3}), 7.85 (dd, $J = 8.3$, $J = 1.7$, 4H, H^{B2}), 7.44 (d, $J = 1.6$, 2H, H^{A5}), 7.40 (dd, $J = 8.2$, $J = 1.7$, 4H, H^{B3}), 2.74 (s, 6H, H^{MeA}), 2.47 (s, 6H, H^{MeC}), 2.33 (s, 6H, H^{MeC}). $^{13}\text{C}\{^1\text{H}\}$ NMR (126 MHz, CDCl_3) δ /ppm: 165.4 ($\text{C}^{\text{C3/C5}}$), 158.8 ($\text{C}^{\text{C3/C5}}$), 158.7 (C^{A6}), 156.7 (C^{A2}), 149.0 (C^{A4}), 138.1 (C^{B1}), 131.2 (C^{B4}), 129.8 (C^{B3}), 127.8 (C^{B2}), 121.2 (C^{A5}), 116.7 (C^{A3}), 116.3 (C^{C4}), 25.0 (C^{MeA}), 11.8 (C^{MeC}), 11.1 (C^{MeC}). ESI-MS: m/z 527.19 $[\text{M} + \text{H}]^+$ (calc. 527.24). HR ESI-MS: m/z 527.2440 $[\text{M} + \text{H}]^+$ (calc. 527.2440).

[Cu(6)₂][PF₆]

Compound **6** (15 mg, 0.053 mmol, 2 eq.) was dissolved in acetone (0.5 mL) and $[\text{Cu}(\text{MeCN})_4][\text{PF}_6]$ (9.9 mg, 0.027 mmol, 1.0 eq.) was added to the solution. The solution was stirred for 10 min and then Et_2O (3 mL) was added. The precipitate that formed was removed by centrifugation to yield $[\text{Cu(6)}_2][\text{PF}_6]$ as a dark-red solid (17 mg, 0.02 mmol, 83%). No further purification was required. ^1H NMR (500 MHz, acetone- d_6) δ /ppm: 8.87 (dd, $J = 5.1$, $J = 1.2$, 2H, H^{A6}), 8.21 (td, $J = 8.0$, $J = 1.6$, 2H, H^{A3}), 8.16 (dd, $J = 7.9$, $J = 1.6$, 2H, H^{A4}), 8.02 (s, 2H, H^{C1}), 7.77 (m, 2H, H^{A5}), 7.75–7.72 (overlapping m, 4H, $\text{H}^{\text{B4+C5}}$), 7.67 (m, 2H, H^{C3}), 7.64 (m, 2H, H^{B3}), 7.54 (m, 2H, H^{B5}), 7.64 (m, 2H, H^{C6}), 7.41 (d, $J = 8.4$, 2H, H^{C4}), 7.36 (ddd, $J = 8.1$, $J = 6.8$, $J = 1.2$, 2H, H^{C7}), 7.24 (d, $J = 8.1$, 2H, H^{C8}). $^{13}\text{C}\{^1\text{H}\}$ NMR (126 MHz, acetone- d_6) δ /ppm: 157.9 (C^{B6}), 153.2, (C^{A2}) 152.9 (C^{B2}), 149.6 (C^{A6}), 138.8 ($\text{C}^{\text{A4+B4}}$), 137.7 (C^{C2}), 134.1 (C^{C4a}), 133.1 (C^{C8a}), 128.8 (C^{C8}), 128.4 ($\text{C}^{\text{C4/C5}}$), 128.3 ($\text{C}^{\text{C4/C5}}$), 127.9 ($\text{C}^{\text{C1/C6}}$), 127.8 ($\text{C}^{\text{C1/C6}}$), 127.3 ($\text{C}^{\text{A5+C7}}$), 125.8 (C^{B5}), 125.3 (C^{C3}), 123.3 (C^{A3}), 120.7 (C^{B3}). UV-vis (CH_2Cl_2 , 2.02×10^{-5} mol dm^{-3}), λ/nm ($\epsilon/\text{dm}^3 \text{ mol}^{-1} \text{ cm}^{-1}$): 235 (103 500), 260 (64 700), 305 (36 600), 430 (5500), 554 (2300). ESI-MS: m/z 627.2 $[\text{M} - \text{PF}_6]^+$ (calc. 627.2). Found C 61.68, H 3.95, N 7.17; $\text{C}_{40}\text{H}_{28}\text{CuF}_6\text{N}_4\text{P}$ requires C 62.14, H 3.65, N 7.25.

[Cu(7)₂][PF₆]

Compound **7** (15 mg, 0.038 mmol, 2 eq.) was dissolved in acetone (0.5 mL) and $[\text{Cu}(\text{MeCN})_4][\text{PF}_6]$ (5.31 mg, 0.019 mmol, 1.0 eq.) were added to the solution. The solution was stirred for 10 min and then Et_2O (3 mL) was added. The precipitate that formed was separated by centrifuge to yield $[\text{Cu(7)}_2][\text{PF}_6]$ as a red solid (14 mg, 0.010 mmol, 78%). No further purification was required. ^1H NMR (500 MHz, acetone- d_6) δ /ppm: 9.15 (d, $J = 1.6$, 4H, H^{A3}), 8.20 (dd, $J = 8.1$, $J = 1.7$, 8H, H^{B2}), 8.11 (d, $J = 1.5$, 4H, H^{A5}), 7.66 (d, $J = 8.1$, $J = 1.7$, 8H, H^{B3}), 2.52 (s, 12H, H^{MeA}), 2.48 (s, 12H, H^{MeC}), 2.31 (s, 12H, H^{MeC}). $^{13}\text{C}\{^1\text{H}\}$ NMR (126 MHz, acetone- d_6) δ /ppm: 165.4 ($\text{C}^{\text{C3/C5}}$), 158.9 ($\text{C}^{\text{C3/C5}}$), 158.7 (C^{A6}), 153.6 (C^{A2}), 150.7 (C^{A4}), 137.0 (C^{B1}), 133.3 (C^{B4}), 130.8 (C^{B3}), 128.8 (C^{B2}), 124.5 (C^{A5}), 118.8 (C^{A3}), 116.5 (C^{C4}), 25.5 (C^{MeA}), 11.7 (C^{MeC}), 10.9 (C^{MeC}). UV-vis (CH_2Cl_2 , 3.33×10^{-5} mol dm^{-3}) λ/nm ($\epsilon/\text{dm}^3 \text{ mol}^{-1} \text{ cm}^{-1}$): 285 (81 600), 325 (52 200), 495 (12 800).

ESI-MS: m/z 1115.4 $[\text{M} - \text{PF}_6]^+$ (calc. 1115.4). HR ESI-MS: m/z 1115.4013 $[\text{M} - \text{PF}_6]^+$ (calc. 1115.4028). Satisfactory elemental analysis was not obtained.

Functionalization of commercial (non-activated nanoparticles): Procedure A

Ligand **1** (10 mg, 1 eq.) was dissolved in dry DMSO (10 mL). Commercial TiO_2 NPs (48.2 mg, 8.4 TiO_2 eq.) were added to the solution and dispersed with sonication for 10 min. The mixture was stirred at room temperature (*ca.* 295 K) for 48 h. Then the particles were separated by centrifugation (10 min, 9000 rpm) and washed with DMSO (3×5 mL) and EtOH (1×5 mL). The NPs were dried under high vacuum and the white powder was stored under N_2 in a sealed vial.

Activation of commercial nanoparticles

Commercial TiO_2 NPs (1 g) were dispersed in dilute aqueous HNO_3 (15 mL, 13.6%) then the mixture was sonicated for 15 min and stirred for 30 min. The NPs were separated by centrifugation and washed once with water (15 mL). Afterwards the NPs were dispersed through sonication (10 min) in water (20 mL) and stirred overnight. The NPs were separated with centrifugation, washed twice with water (2×20 mL) and then dried over high vacuum. The activated NPs (950 mg) were stored in a sealed vial under N_2 .

Functionalization of activated nanoparticles (Procedure B)

Ligand **1** (3.73 mg, 1 eq.) was placed in a microwave vial and milliQ water (13 mL) was added. The mixture was dispersed by sonication for 1 min. Activated TiO_2 NPs (60.0 mg, 28 TiO_2 eq.) were added to the solution and dispersed with sonication for 10 min. The microwave vial was sealed and the reaction mixture was heated to 130 °C for 3 h in the microwave reactor. The reaction mixture was allowed to cool to room temperature. The functionalized NPs were separated from the solvent by centrifugation (10 min, 9000 rpm). Then the functionalized NPs were dried under high vacuum yielding a slightly yellow powder.

Analogous procedures were used to functionalize activated NPs with ligands **2**, **3** or **4** starting with **2** (2.56 mg, 1 eq.), **3** (2.92 mg, 1 eq.), **4** (3.19 mg, 1 eq.) and activated TiO_2 NPs (60.0 mg, 28 TiO_2 eq.). For **4**, the functionalized NPs were washed with DMSO (3×10 mL) and EtOH (3×10 mL); see discussion in manuscript. The functionalized NPs were dried under high vacuum and the white powder was stored under N_2 in a sealed vial.

Functionalization of activated nanoparticles: competition between anchoring ligands (Procedure C)

Ligands **1** (3.73 mg, 1 eq.) and **2** (2.56 mg, 1 eq.) were placed in a microwave vial and milliQ water (13 mL) was added. The mixture was dispersed by sonication for 1 min. Activated TiO_2 NPs (60.0 mg, 28 TiO_2 eq.) were added to the solution and dispersed with sonication for 10 min. The microwave vial was sealed and the reaction mixture was heated to 130 °C for 3 h in a microwave reactor. The reaction mixture was allowed to cool



to room temperature. The water was then removed under high vacuum and then some of the residue was dispersed in DMSO- d_6 in an NMR tube.

An analogous procedure was used with combinations of ligands **1** (3.73 mg, 1 eq.) and **3** (2.92 mg, 1 eq.), or ligands **1** (3.73 mg, 1 eq.) and **4** (3.19 mg, 1 eq.) with activated TiO₂ NPs (60.0 mg, 28 TiO₂ eq.).

Functionalization of activated nanoparticles: competition between anchoring ligands (Procedure D)

Ligand **4** (3.19 mg, 1 eq.) was placed in a microwave vial and milliQ water (13 mL) was added. The mixture was dispersed by sonication for 1 min. Activated TiO₂ NPs (60.0 mg, 28 TiO₂ eq.) were added to the solution and dispersed with sonication for 10 min. The microwave vial was sealed and the reaction mixture was heated to 130 °C for 3 h in the microwave reactor. The reaction mixture was allowed to cool to room temperature. The water was then removed under high vacuum and then some of the residue was dispersed in DMSO- d_6 in an NMR tube and the ¹H NMR spectrum was recorded. The remaining residue was washed by dispersing it in DMSO (3 × 10 mL) and EtOH (3 × 10 mL). The washed residue was collected by centrifugation and was dried under high vacuum. Then some of the residue was dispersed in DMSO- d_6 . The NMR spectrum revealed that no excess free ligand was left on the functionalized NPs. Ligand **1** (2.49 mg, 1 eq.) was placed in a microwave vial and milliQ water (13 mL) was added. The mixture was dispersed by sonication for 1 min. The previously obtained NPs functionalized with **4** (40 mg) were added to the solution and dispersed with sonication for 10 minutes. The microwave vial was sealed and the reaction mixture was heated to 130 °C for 3 h in the microwave reactor. The reaction mixture was allowed to cool to room temperature. The water was then removed under high vacuum to yield a residue, a portion of which was dispersed in DMSO- d_6 in an NMR tube.

Complexation of nanoparticles functionalized with anchored ligands

Stock solutions of [Cu(MeCN)₄][PF₆]₄ (5.59 mg, 10 mL, 1.5 mM in acetone) and FeCl₂·4H₂O (2.88 mg, 10 mL, 1.5 mM in acetone) were prepared.

Activated NPs functionalized with ligands (10 mg) (Procedures B or C above) were dispersed by sonication (15 s) in water (1.35 mL) and the stock solution of [Cu(MeCN)₄][PF₆]₄ in the case of **1**, **2** or **4** (0.15 mL) or of FeCl₂·4H₂O in the case of **3** (0.15 mL) was added. The solutions in the sample vials were stirred for 72 h. The coloured NPs were separated by centrifugation (10 min, 13 200 rpm), then washed with acetone (3 × 1 mL) and dried under high vacuum.

SALSAC assembly of heteroleptic copper(i) complexes on activated nanoparticles

Stock solutions of [Cu(5)₂][PF₆]₂, [Cu(6)₂][PF₆]₂ and [Cu(7)₂][PF₆]₂ (1.5 mM in acetone) were prepared. NPs functionalized with **1** (10 mg, see Procedure B) were dispersed in water (1.35 mL) by sonication (15 s) and then a portion (0.15 mL) of the stock

solution of [Cu(5)₂][PF₆]₂ was added. The mixture was stirred for 72 h. The orange-red NPs were separated from the supernatant liquid by centrifugation (10 min, 13 200 rpm), then washed with acetone (3 × 1 mL) and dried under high vacuum. The procedure was repeated using [Cu(6)₂][PF₆]₂ or [Cu(7)₂][PF₆]₂.

SALSAC assembly of heteroleptic iron(II) complexes on activated nanoparticles

A stock solution of [Fe(8)₂][PF₆]₂ (1.5 mM in acetone) was prepared. NPs functionalized with **3** (10 mg, see Procedure B) were dispersed in water (1.35 mL) by sonication (15 s) and then a portion (0.15 mL) of the stock solution of [Fe(8)₂][PF₆]₂ was added. The mixture was stirred for 72 h. The purple NPs were separated from the supernatant liquid by centrifugation (10 min, 13 200 rpm), then washed with acetone (3 × 1 mL) and dried under high vacuum.

Results and discussion

Choice of anchoring ligands

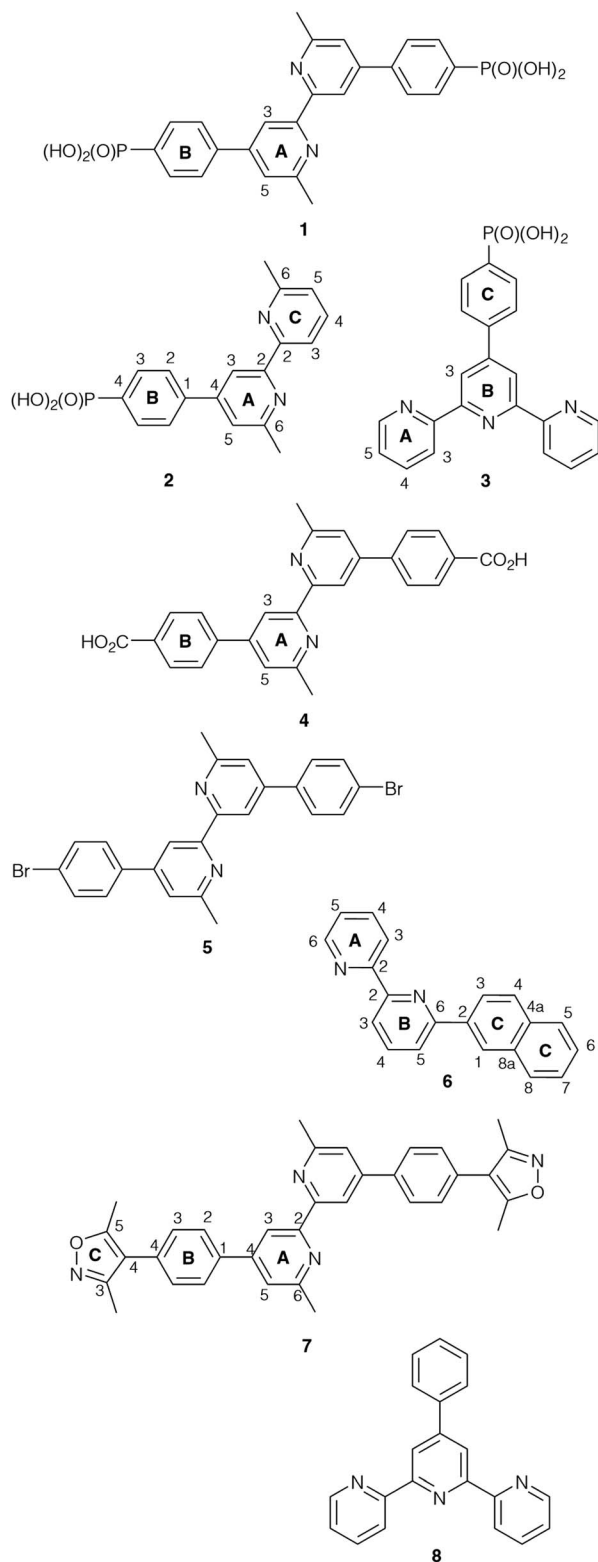
Based on our previous experience of functionalizing TiO₂ surfaces,^{19,20,24} anchoring ligands **1** and **4** (Scheme 1) were selected for the present investigation to provide a comparison of carboxylic *versus* phosphonic acid anchors. The DSC community consider that phosphonic acid anchors give more stable attachment to TiO₂ surfaces than carboxylic acids.⁴⁹ Both **1** and **4** contain a bpy metal-binding domain for coordination to copper(i).¹⁹ The presence of the 6,6'-dimethyl substituents stabilizes a bis(diimine)copper(i) complex against oxidation by inhibiting a geometrical change from tetrahedral (favoured by Cu⁺) to square planar (favoured by Cu²⁺).^{50,51} Ligand **2** was designed to allow a comparison of mono- *versus* bis(phosphonic acid) anchors (**2** *versus* **1**) bearing the same bpy metal-binding domains. Both **2** and **3** carry one phosphonic acid group, but differ in the metal-binding unit; bpy and 2,2':6',2''-terpyridine (tpy) can be addressed by copper(i) and iron(II), respectively. Each of ligands **1**–**4** contains a phenylene spacer between the anchoring group and the metal-binding units.

Compound **2** was prepared as described in the Experimental section. The base peak in the electrospray mass spectrum at *m/z* 339.06 (Fig. S1†) was assigned to [M – H][–]. The ¹H and ¹³C NMR spectra of **2** (Fig. S2 and S3†) were assigned by COSY, NOESY, HMQC and HMBC methods (Fig. S4–S6†) and were consistent with the structure shown in Scheme 1.

Nanoparticle activation and general procedure for functionalization

Our initial attempts to replicate TiO₂ surface-functionalization using commercial NPs (AEROXIDE TiO₂ P25) suspended in DMSO in place of screen-printed and annealed (commercial or in-house fabricated) surfaces following previously published protocols^{20,52} met with variable success. A significant observation came from DOSY experiments on a DMSO- d_6 solution of **1** and a DMSO- d_6 suspension of dried commercial NPs after treatment with **1** (Procedure A in the Experimental section). Fig. 2 shows a comparison of the ¹H NMR spectra of the two





Scheme 1 Structures of compounds 1–8. Atom numbering schemes are given where required for NMR spectroscopic assignments.

samples. Apart from small changes (<0.1 ppm) in the chemical shifts of signals, the spectra are essentially identical and the signals remain sharp. This strongly suggests that free ligand **1** is

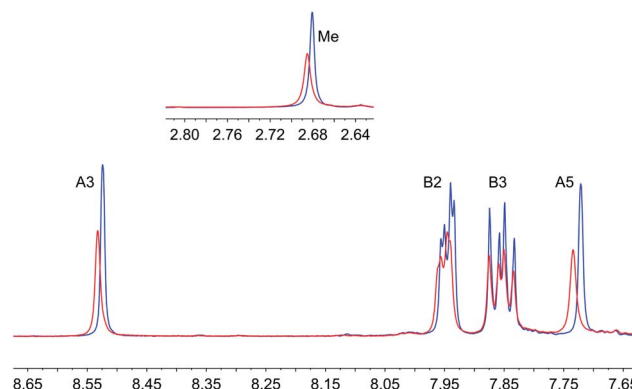


Fig. 2 ¹H NMR spectrum (500 MHz, DMSO-*d*₆, aromatic region with methyl region inset) of **1** (blue) and of the NPs after treatment with **1** following Procedure A in Experimental section (red). Chemical shifts in δ/ppm.

present in the solution containing dispersed NPs. To unambiguously confirm this proposal, PFGSE spectra of **1** before and after exposure to commercial NPs were recorded. The proton signal at δ 8.525 ppm was selected to determine the diffusion coefficient by a two-parameter fit to the DOSY intensities. For **1** in DMSO-*d*₆, a diffusion coefficient of $1.355 \times 10^{-10} \text{ m}^2 \text{ s}^{-1}$ was determined (Fig. S7a†), and for the solution containing the dispersed NPs the diffusion coefficient was $1.326 \times 10^{-10} \text{ m}^2 \text{ s}^{-1}$ (Fig. S7b†), identical to the previous value within experimental error. These data are consistent with either some or all of **1** remaining non-anchored during attempts to functionalize the NPs using Procedure A detailed in the Experimental section. This illustrates a general problem with non-activated NPs, that simple washing does not suffice to remove surface-adsorbed or aggregated ligand from NPs with anchored ligand.

We therefore decided to *activate* the commercial TiO₂ NPs prior to *functionalization* with the ligand. Literature activation procedures⁵³ include treatment with HNO₃ (ref. 54) and ultrasound sonication for to optimize particle dispersion.⁵⁵ Initial tests revealed that replacing DMSO by water was advantageous for NP functionalization, and that reducing the amount of anchoring ligand with respect to the quantity of NPs was also beneficial. We therefore modified the procedure by an initial treatment of the commercial NPs with aqueous HNO₃ (see Experimental section). Following this, the activated NPs were added to an aqueous suspension of **1**, **2**, **3** or **4** and dispersed with sonication before the suspension was heated at 130 °C for 3 h under microwave conditions before being separated from the solvent by centrifugation (see Procedure B in the Experimental section). Fig. 3 compares part of the FT-IR spectra of the activated NPs, free ligand **1** and activated NPs functionalized with **1**; the full spectra are given in Fig. S8.† The spectrum of the functionalized NPs exhibits bands at 1629, 1601, 1570 and 1545 cm⁻¹. While the bands appear to be characteristic of free ligand **1**, closer inspection of Fig. 3 shows differences with the spectroscopic signature of pristine **1** which has absorptions at 1645, 1624, 1598 and 1545 cm⁻¹. Significantly, this pattern of absorptions is retained in a mixture of commercial NPs (non-



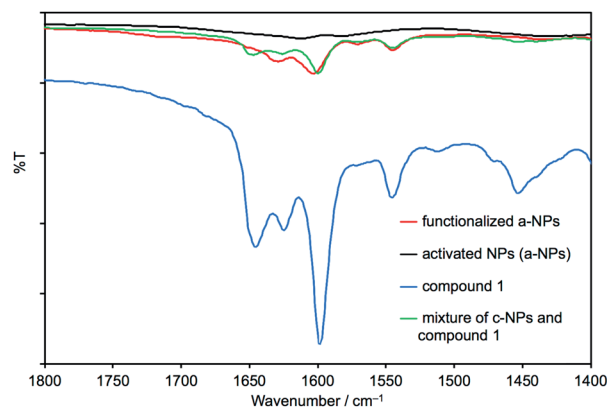


Fig. 3 Solid-state IR spectra of activated NPs (a-NPs), pristine **1**, a-NPs functionalized with **1** following Procedure B in the Experimental section, and a mixture of commercial NPs (c-NPs) and **1**. The full IR spectra are presented in Fig. S8†

activated) and **1** (1647, 1624, 1600 and 1543 cm^{-1} , Fig. 3). Thus, the IR spectroscopic data provide evidence that ligand **1** is anchored to the TiO_2 . A comparison of the IR spectra of ligand **3** and NPs functionalized with **3** is shown in Fig. S9†. Thermogravimetric analysis (TGA) of the activated NPs and those functionalized with **1** was carried out, and the results are displayed in Fig. 4. Both samples show a weight loss of about 2% in two steps (isotherm maxima $<120^\circ\text{C}$ and $<330^\circ\text{C}$) attributed to the loss of physisorbed and chemisorbed water, respectively. The non-functionalized NPs undergo no further change in mass, even after being heated at 900°C for 30 minutes. In contrast, the NPs functionalized with **1** exhibit a further 2% weight loss above *ca.* 430°C ascribed to decomposition of the ligand. The profile of the TGA curve above 430°C (red curve in Fig. 4) is similar to that of the thermal decomposition of **1** (Fig. S10†). Three measurements were made for the functionalized NPs to confirm reproducibility of the data.

Further evidence for NP functionalization came from a comparison of the ^1H NMR spectra of the pristine ligands **1**, **2** or **3** in $\text{DMSO}-d_6$ with those of suspended NPs functionalized with **1**, **2** or **3** (Fig. 5, S11 and S12†). The functionalized NPs were prepared according to Procedure B in the Experimental section.

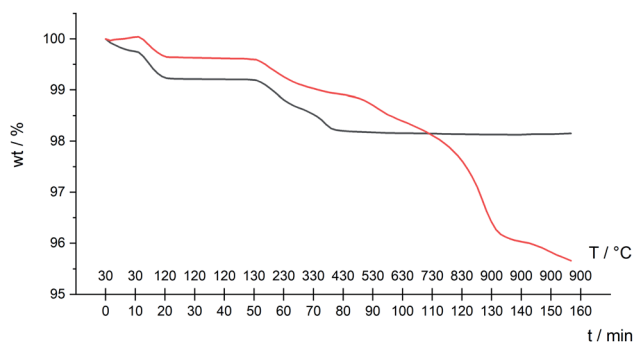


Fig. 4 TGA curves for activated NPs only (black line), and activated NPs functionalized with **1** following Procedure B in the Experimental section (red line).

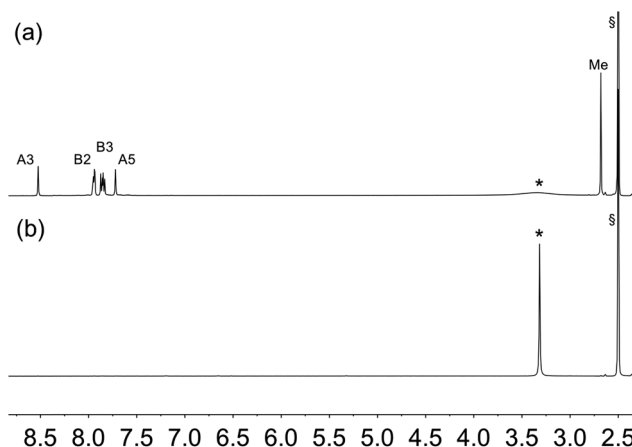


Fig. 5 ^1H NMR (500 MHz, $\text{DMSO}-d_6$, 298 K) of (a) ligand **1** and (b) suspended residue after activated TiO_2 NPs had been after activated TiO_2 NPs were functionalized with **1** following Procedure B in Experimental section, separated by centrifugation and dried. See Scheme 1 for atom labelling. Chemical shifts in δ/ppm . § = residual $\text{DMSO}-d_5$. * = water.

After centrifugation and drying, the functionalized NPs were not washed. The ligand anchored to the NP is NMR silent, and Fig. 5b confirms that all of ligand **1** (shown to be present in the IR study of the same material) is anchored to the TiO_2 surface. In the case of ligand **4**, the bulk residue showed a signal due to free **4** and the material had to be thoroughly washed with DMSO and EtOH to completely remove traces of free ligand (Fig. S13†). This indicates that the carboxylic acid anchoring ligand **4** adsorbed less efficiently to the surface of the TiO_2 NPs than the phosphonic acids **1**, **2** and **3**. We return to this later.

To confirm that the functionalized NPs bear anchored ligands capable of coordination to metal ions, NPs functionalized as described above with **1**, **2**, **3** or **4** were dispersed in water by sonication and an acetone solution of $[\text{Cu}(\text{MeCN})_4][\text{PF}_6]$ (for **1**, **2** and **4**) or $\text{FeCl}_2 \cdot 4\text{H}_2\text{O}$ (for **3**) was added. Colour changes were observed after about five minutes and the intensity of colour increased over a period of an hour (Fig. 6 and S14†). The orange and purple colours are, respectively, characteristic of

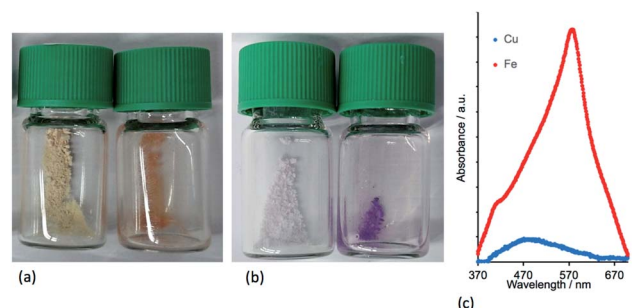


Fig. 6 Photographs of (a) activated TiO_2 NPs functionalized with **1** (left) and after treatment with $[\text{Cu}(\text{MeCN})_4][\text{PF}_6]$ (right), and (b) activated TiO_2 NPs functionalized with **3** (left) and after treatment with $\text{FeCl}_2 \cdot 4\text{H}_2\text{O}$ (right). (c) Solid-state absorption spectra of the NPs functionalized with **1** or **3** and treated with $[\text{Cu}(\text{MeCN})_4][\text{PF}_6]$ (blue curve) and $\text{FeCl}_2 \cdot 4\text{H}_2\text{O}$ (red).



$[\text{Cu}(\text{diimine})_2]^+$ and $[\text{Fe}(\text{tpy})_2]^{2+}$ chromophores, and imply that addition of the metal ion results in coordination by two adjacent ligands on a single NP or two ligands on adjacent NPs. Solid-state absorption spectra of the samples (Fig. 6c) exhibit metal-to-ligand charge transfer (MLCT) bands at 489 and 579 nm which, along with the band profiles, are typical of $[\text{Cu}(\text{diimine})_2]^+$ and $[\text{Fe}(\text{tpy})_2]^{2+}$ chromophores, respectively. Scanning electron microscopy (SEM) was used to image the TiO_2 NPs before (Fig. 7a) and after functionalization with **1** and $[\text{Cu}(\text{MeCN})_4][\text{PF}_6]$ (Fig. 7b). The 'halo' around each NP in Fig. 7b is interpreted as the sheath of organic ligand **1**. The dimensional relationship between the TiO_2 NP and the 'halo' supports this proposal.

The ligand-functionalized NPs can be stored as dry solids under N_2 for periods of months without loss of activity.

Competition between different pairs of anchors on NPs

In applying the SALSAC approach to DSCs, we have demonstrated that devices incorporating dyes with phosphonic acid anchors outperform those with analogous dyes with carboxylic acid anchors.^{56,57} Similarly, Grätzel and coworkers have observed strong surface adhesion of ruthenium(II) dyes bearing phosphonic acid anchoring groups.⁵⁸ Despite this latter finding being reported as early as 1995, the DSC community continues to favour the use of carboxylic acid anchoring units.

We decided to investigate the competitive binding to TiO_2 NPs of pairs of ligands **1** and **3**, **1** and **4**, and **1** and **2** to gain insight into preferential binding of phosphonic and carboxylic acid anchors, and competition between spatially different ligands bearing phosphonic acids. Equimolar amounts of each pair of ligands (**1** and **3**, **1** and **4**, or **1** and **2**) were added to water and then TiO_2 NPs, activated as described above were added and dispersed with sonication (see Procedure C in the Experimental section). Each mixture was heated to 130 °C for 3 hours in a microwave reactor. After cooling and removal of water *in*

vacuo, part of the residue was dispersed in $\text{DMSO}-d_6$ in an NMR tube and ^1H NMR spectra of the suspended residues were then recorded. Once again, ligands anchored to the NP surface will not be observed. Fig. 8 displays the ^1H NMR spectra of pristine ligands **1**, **3** (Fig. 8a and b) and the suspended residue after activated NPs had been treated with a 1 : 1 molar mixture of **1** and **3** (Fig. 8c). Signals in Fig. 8c are attributed to ligands that are not bound to the surface. Fig. 8c shows both free ligands **1** and **3** in solution, and the small changes in chemical shifts on going from Fig. 8a or 8b to 8c are consistent with those described in the previous section. The molar ratio of ligands **1** : **3** in the solution investigated in Fig. 8c is 2 : 1 based on the relative integrals of the signals for protons H^{A3} and H^{A5} in each ligand (see Scheme 1 and Fig. 8c). This indicates that the TiO_2 NPs preferentially bind **3**. Three portions of the washed and dried functionalized NPs (shown to contain no free ligand, Fig. 8d) were dispersed in water by sonication and an acetone solution of $[\text{Cu}(\text{MeCN})_4][\text{PF}_6]$ was added to one portion, an acetone solution of both $[\text{Cu}(\text{MeCN})_4][\text{PF}_6]$ and $\text{FeCl}_2 \cdot 4\text{H}_2\text{O}$ to the second, and an acetone solution of $\text{FeCl}_2 \cdot 4\text{H}_2\text{O}$ to the third. Fig. 9a shows the visual difference between the samples, but definitive evidence that both **1** and **3** are bound to the surface comes from a comparison of the IR spectra (Fig. 9b) of NPs functionalized with **1**, with **3** or after activated TiO_2 NPs were functionalized with a 1 : 1 mixture of **1** and **3** following Procedure C in the Experimental section. The IR spectrum of the latter exhibits diagnostic absorptions of both ligands.

Next, we investigated the functionalization of TiO_2 NPs with a 1 : 1 molar mixture of **1** and **2**. Both ligands contain a 6,6'- Me_2bpy unit, but ligand **1** contains two phosphonic acid groups while **2** contains one (Scheme 2). In the ^1H NMR spectrum of the suspension of functionalized NPs in $\text{DMSO}-d_6$ (Fig. S15c†) the ratio of integrals of signals for protons H^{A3} (or of H^{A5}) of each ligand in solution is *ca.* 1 : 1. This is consistent with there being approximately twice as much **2** as **1** remaining in solution after activated TiO_2 NPs have been treated with a 1 : 1 mixture of **1** and **2**. Thus, **1** is preferentially bound to the surface.

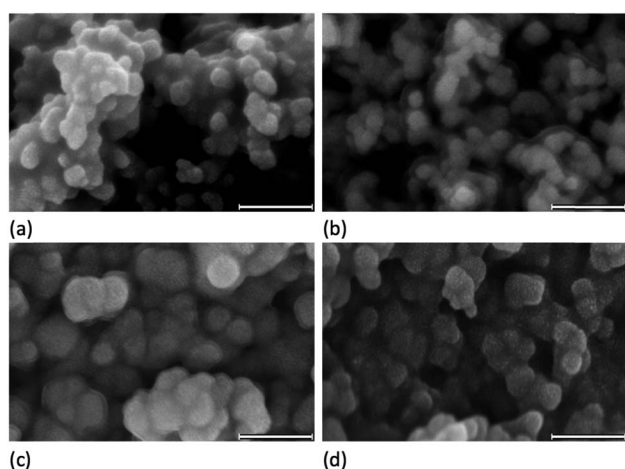


Fig. 7 SEM images of (a) activated TiO_2 NPs, and (b) activated TiO_2 NPs functionalized with **1** and treated with $[\text{Cu}(\text{MeCN})_4][\text{PF}_6]$. Activated TiO_2 NPs functionalized with **1** and after treatment with (c) $[\text{Cu}(\text{5})_2][\text{PF}_6]$ or (d) $[\text{Cu}(\text{7})_2][\text{PF}_6]$. Each scale bar = 100 nm.

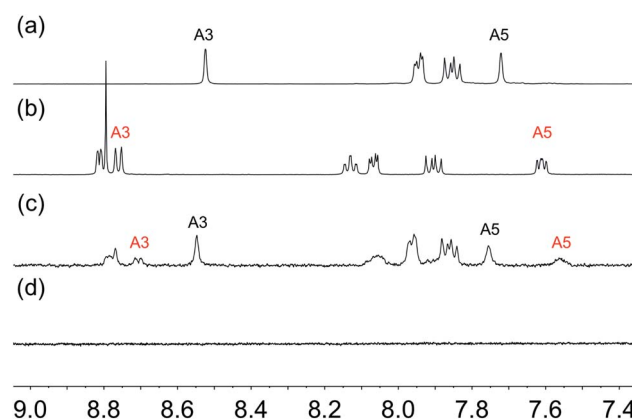


Fig. 8 Aromatic regions of the ^1H NMR (500 MHz, $\text{DMSO}-d_6$, 298 K) of (a) ligand **1**, (b) ligand **3**, (c) suspended residue after activated TiO_2 NPs were functionalized with **1** and **3** following Procedure C in the Experimental section, (d) residue after washing. See Scheme 1 for atom labelling. Chemical shifts in δ/ppm .



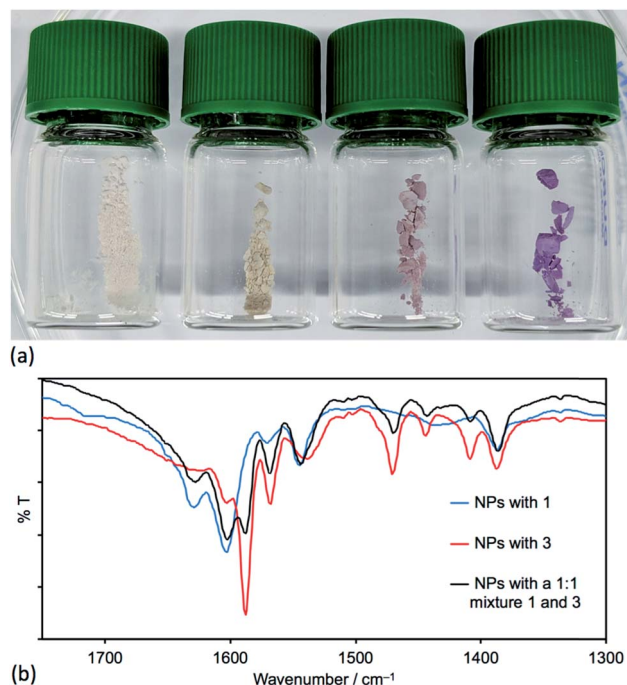
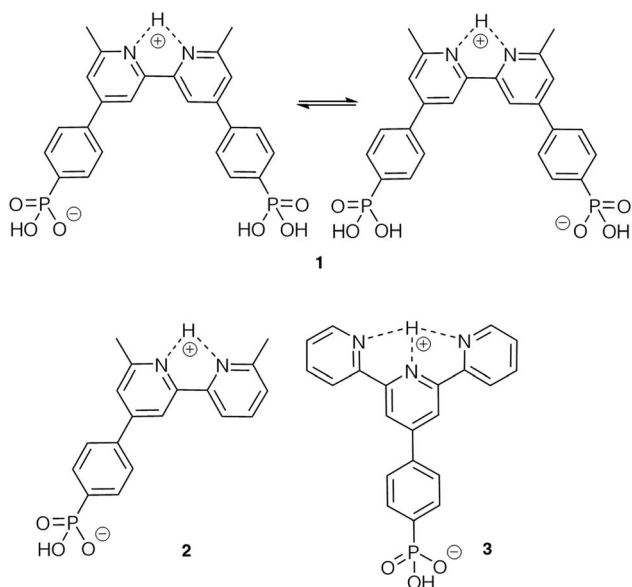


Fig. 9 (a) Photographs of (left to right) activated TiO_2 NPs after functionalized with a 1 : 1 mixture of **1** and **3**, after one portion has been further treated with $[\text{Cu}(\text{MeCN})_4][\text{PF}_6]$, after another portion has been further treated with $[\text{Cu}(\text{MeCN})_4][\text{PF}_6]$ and $\text{FeCl}_2 \cdot 4\text{H}_2\text{O}$, and after a final portion has been further treated with $\text{FeCl}_2 \cdot 4\text{H}_2\text{O}$. (b) Solid-state FT-IR spectra of NPs functionalized with ligand **1** only, with **3** only, and activated TiO_2 NPs functionalized with **1** and **3** following Procedure C in the Experimental section.

In order to rationalize the results of the competition experiments, it is pertinent to note that we have previously demonstrated that in $\text{DMSO}-d_6$, ligand **1** exists as a zwitterion.³¹ This is consistent with known values of $\text{pK}_a = 4.4$ for $[\text{Hbpy}]^+$,⁵⁹ and of



Scheme 2 Zwitterionic structures of ligands **1**–**3**.

$\text{pK}_a(\mathbf{1}) = 1.86$ for $\text{PhPO}(\text{OH})_2$.⁶⁰ On the other hand, the 6,6'-dimethyl substituents in **1** will render the Me_2bpy unit a weaker base than bpy, as is observed for 1,10-phenanthroline (pK_a for $[\text{Hphen}]^+ = 4.86$ (ref. 61)) and 2,9-dimethyl-1,10-phenanthroline (pK_a for $[\text{HMe}_2\text{phen}]^+$ is reported as 5.85 (ref. 62) and 6.17 (ref. 61)). The zwitterionic form of **1** should exhibit a *cis*-configuration arising from hydrogen bonding⁶³ (Scheme 2). Similarly, we expect **2** to exist as a zwitterion in water and DMSO (Scheme 2). Values of $\text{pK}_a = 4.54$ and 3.57 for $[\text{Htpy}]^+$ and $[\text{H}_2\text{tpy}]^{2+}$ (measured in 0.2 M aqueous KCl at 298 K)⁶⁴ indicate that **3** is also likely to show zwitterionic behaviour (Scheme 2), as has also been reported for 2,2':6',2''-terpyridin-4'-ylphosphonic acid.⁶⁵ We expect the availability of phosphonate groups in the zwitterionic forms of the ligands to favour surface binding³¹ and the observed binding orders of $\mathbf{3} > \mathbf{1} > \mathbf{2}$ can be rationalized in terms of the relative pK_a values and the number of anchoring groups in the ligands.

When activated TiO_2 NPs were treated under microwave conditions with a 1 : 1 mixture of ligands **1** and **4**, we observed that only carboxylic acid **4** remained in solution (Fig. 10). The strong adsorption of the phosphonic acid **1** to NPs dispersed in solution is consistent with what we and Grätzel have observed for annealed TiO_2 surfaces.^{56–58} The preferential binding of **1** with respect to **4** was also demonstrated by ligand displacement. Activated TiO_2 NPs were dispersed in an aqueous suspension of **4** and then heated under microwave conditions at 130°C for 3 hours. After cooling, the water was removed, and part of the residue was suspended in $\text{DMSO}-d_6$. Sharp signals in the ^1H NMR spectrum were consistent with the presence of non-anchored ligand (Fig. 10a). The remaining residue was thoroughly washed until, NMR analysis of a part of the residue dispersed in $\text{DMSO}-d_6$ revealed no signal for free ligand **4** (Fig. 11b). We demonstrated that some **4** ligand remained and was surface-bound by treating the residue with $[\text{Cu}(\text{MeCN})_4][\text{PF}_6]$. The observation of an orange colour (see the photograph in Fig. 11) is characteristic of the formation of a $[\text{Cu}(\text{diimine})_2]^+$ chromophore (see earlier). The functionalized NPs were then treated with **1** in aqueous solution under microwave conditions (see Procedure C in the Experimental

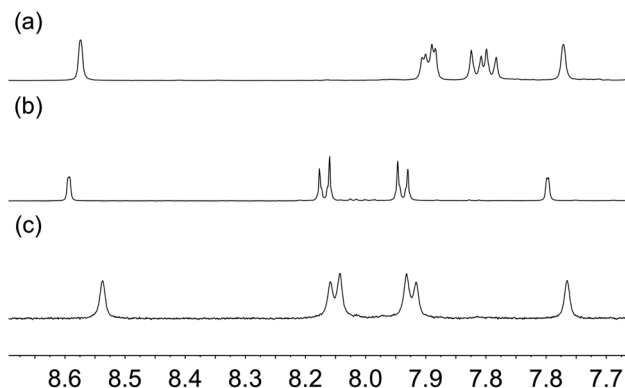


Fig. 10 ^1H NMR (500 MHz, $\text{DMSO}-d_6$, 298 K) of (a) ligand **1**, (b) ligand **4**, (c) suspended residue after activated TiO_2 NPs had been treated with a 1 : 1 mixture of **1** and **4** following Procedure C in the Experimental section.



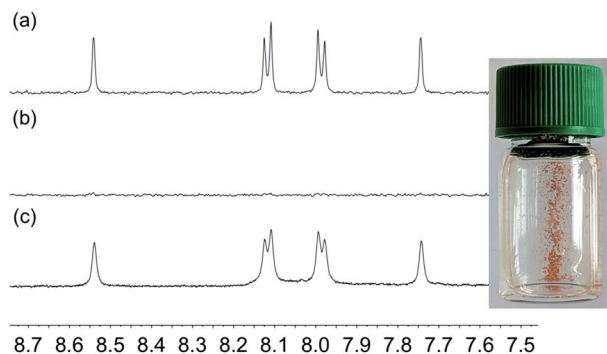
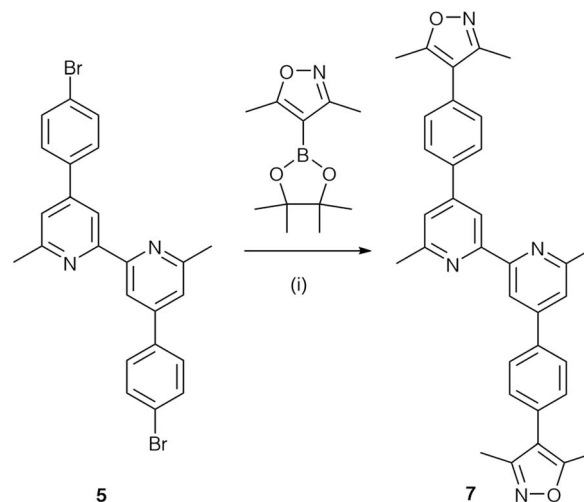


Fig. 11 ^1H NMR (500 MHz, $\text{DMSO}-d_6$, 298 K) of (a) suspended residue after activated TiO_2 NPs had been treated with **4**, (b) suspended residue after thorough washing (see text), and (c) suspended residue after NPs functionalized with **4** had been treated with **1** following Procedure D in the Experimental section. Chemical shifts in δ/ppm . The photograph shows the residue from (b) after treatment with $[\text{Cu}(\text{MeCN})_4][\text{PF}_6]$ (see text).

section). After removal of water, the residue was analysed by ^1H NMR spectroscopy (Fig. 11c). The spectrum exhibited sharp signals with the signature of ligand **4**. No free ligand **1** (compare with Fig. 10a) was observed, confirming the displacement of surface-bound **4** by **1**.

Application of SALSAC: preparation and characterization of homoleptic copper(i) complexes

To test the application of the SALSAC approach to the functionalization of NPs, we first prepared the homoleptic compounds $[\text{Cu}(\text{L}_{\text{ancillary}})_2][\text{PF}_6]$ and $[\text{Fe}(\mathbf{8})_2][\text{PF}_6]_2$. The iron(II) complex was prepared as previously described.⁴⁷ The general method for the copper(i) complexes was the reaction of $[\text{Cu}(\text{MeCN})_4][\text{PF}_6]$ with two equivalents of $\text{L}_{\text{ancillary}}$ followed by precipitation of $[\text{Cu}(\text{L}_{\text{ancillary}})_2][\text{PF}_6]$. $[\text{Cu}(\mathbf{5})_2][\text{PF}_6]$ has previously been described.⁴⁴ Reaction of ligand **6** (ref. 45) with $[\text{Cu}(\text{MeCN})_4][\text{PF}_6]$ yielded $[\text{Cu}(\mathbf{6})_2][\text{PF}_6]$. Ligand **7** was prepared as shown in Scheme 3 and was characterized by ^1H and ^{13}C NMR spectroscopy (Fig. S16–S19[†]) with assignment of the signals by 2D methods (see Experimental section), electrospray MS (Fig. S20[†]) and IR spectroscopy (Fig. S21[†]). $[\text{Cu}(\mathbf{7})_2][\text{PF}_6]$ was isolated as a red solid. The ESI mass spectra of $[\text{Cu}(\mathbf{6})_2][\text{PF}_6]$ and $[\text{Cu}(\mathbf{7})_2][\text{PF}_6]$ showed peaks at m/z 627.2 $[\text{M} - \text{PF}_6]^+$ and 1115.4, respectively, arising from the $[\text{M} - \text{PF}_6]^+$ ion. The ^1H and ^{13}C $\{^1\text{H}\}$ NMR spectra of $[\text{Cu}(\mathbf{6})_2][\text{PF}_6]$ and $[\text{Cu}(\mathbf{7})_2][\text{PF}_6]$ were assigned by COSY, NOESY, HMQC and HMBC methods and selected spectra are shown in Fig. S22–S28.[†] The solid-state IR spectra of the compounds (Fig. S29[†]) exhibit a characteristic strong absorption at 833 cm^{-1} from the $[\text{PF}_6]^-$ ion. The solution absorption spectra of the two compounds (Fig. 12) exhibit intense absorption bands below *ca.* 340 nm arising from spin-allowed ligand-centred $\pi^* \leftarrow \pi$ transitions. The broad absorption band centred at 495 nm in $[\text{Cu}(\mathbf{7})_2][\text{PF}_6]$ is assigned to an MLCT transition and is typical of homoleptic bis(diimine)copper(i) complexes in which the 6,6'-substituents are methyl groups.^{19,66} In contrast, $[\text{Cu}(\mathbf{6})_2][\text{PF}_6]$ exhibits two bands at 430 and 554 nm which are reminiscent of those



Scheme 3 Synthetic route to compound **7**. Conditions: (i) Cs_2CO_3 , catalytic amount of $[\text{Pd}(\text{PPh}_3)_4]$, toluene, 110°C , 4 h in a microwave reactor; isolated in 33% yield.

at 423 and 573 nm in $[\text{CuL}_2][\text{PF}_6]$ where $\text{L} = 4,4'$ -bis(4-bromophenyl)-6,6'-diphenyl-2,2'-bipyridine.⁴⁴ The profile of the spectrum and the red-shift in absorption maximum are consistent with the effects of introducing phenyl substituents adjacent to the nitrogen donors in $[\text{Cu}(\text{dpp})_2]^+$ ($\text{dpp} = 2,9$ -diphenyl-1,10-phenanthroline),^{67,68} and have been attributed to the flattened, low-symmetry structure of the complex.⁶⁸

Application of SALSAC: NPs functionalized with heteroleptic copper(i) and iron(II) complexes

Route 2 in Fig. 1 summarized the SALSAC approach for TiO_2 surface modification using ligand exchange between a surface-anchored ligand and one ligand from a homoleptic bis(diimine) copper(i) complex to produce a surface functionalized with a heteroleptic copper(i) complex (eqn (1)).

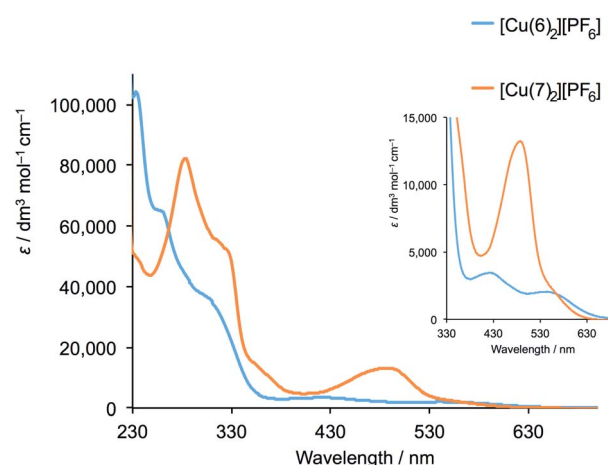


Fig. 12 Solution absorption spectra of $[\text{Cu}(\mathbf{6})_2][\text{PF}_6]$ ($2.02 \times 10^{-5}\text{ mol dm}^{-3}$) and $[\text{Cu}(\mathbf{7})_2][\text{PF}_6]$ ($3.33 \times 10^{-5}\text{ mol dm}^{-3}$) in CH_2Cl_2 . The inset shows an expansion of the MLCT region.

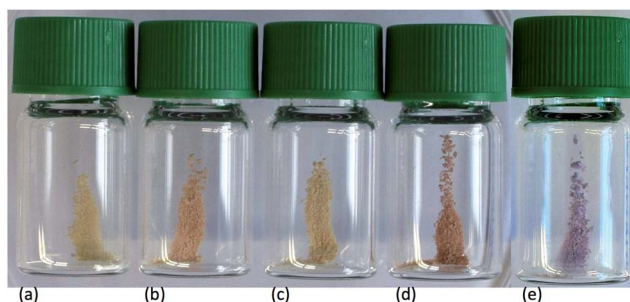
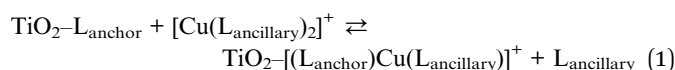


Fig. 13 Photographs of activated TiO_2 NPs functionalized (a) with **1**, and after treatment with (b) $[\text{Cu}(5)_2][\text{PF}_6]$, (c) $[\text{Cu}(7)_2][\text{PF}_6]$, (d) $[\text{Cu}(6)_2][\text{PF}_6]$ and (e) $[\text{Fe}(8)_2][\text{PF}_6]_2$.



To date, we have applied this strategy to annealed nanoparticulate TiO_2 surfaces, and we now demonstrate an extension to TiO_2 NPs dispersed in solution. NPs functionalized with **1** were dispersed in water, and an acetone solution of $[\text{Cu}(5)_2][\text{PF}_6]$, $[\text{Cu}(6)_2][\text{PF}_6]$ or $[\text{Cu}(7)_2][\text{PF}_6]$ was added (see Experimental section). During a 72 hour period of stirring, the NPs became orange-red. A similar procedure was followed for ligand exchange between $[\text{Fe}(8)_2][\text{PF}_6]_2$ and NPs functionalized with **3** which resulted in purple-coloured NPs. The NPs were separated by centrifugation, and were washed and dried. The observed colours of the NPs (Fig. 13) are diagnostic of $[\text{Cu}(\text{diimine})_2]^+$ and $[\text{Fe}(\text{tpy})_2]^{2+}$ chromophores, and their solid-state absorption spectra are shown in Fig. 14 and S30.† Absorption maxima are observed at 491, 498 and 488 nm for the copper(i) complexes with $\text{L}_{\text{ancillary}} = 5, 6$ and **7**, respectively, and at 577 nm for the surface bound iron(ii) complex. That the latter arise from ligand exchange and not from residual homoleptic complexes is best demonstrated by comparing the solid-state spectrum of NPs functionalized with **1** after treatment with $[\text{Cu}(6)_2][\text{PF}_6]$ with that of the homoleptic $[\text{Cu}(6)_2][\text{PF}_6]$. As discussed earlier, significant red-shifting is observed in the solution absorption spectrum of $[\text{Cu}(6)_2][\text{PF}_6]$ due to flattening of the copper(i)

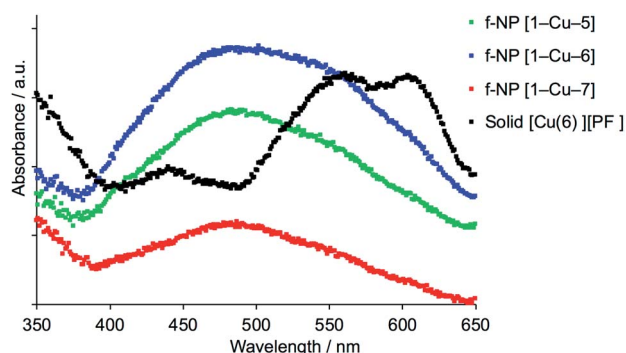


Fig. 14 Solid-state absorption spectra of NPs functionalized with **1** after treatment with $[\text{Cu}(5)_2][\text{PF}_6]$, $[\text{Cu}(6)_2][\text{PF}_6]$ or $[\text{Cu}(7)_2][\text{PF}_6]$, and, for comparison, the solid-state absorption spectrum of homoleptic $[\text{Cu}(6)_2][\text{PF}_6]$.

coordination sphere, and this is also observed in the solid-state with an MLCT band centred at *ca.* 580 nm (Fig. 14).

SEM images of the TiO_2 NPs functionalized with **1** after treatment with $[\text{Cu}(5)_2][\text{PF}_6]$ and $[\text{Cu}(7)_2][\text{PF}_6]$ are displayed in Fig. 7c and d. Comparison with the images in Fig. 7a and b reveals an increase in particle size after reaction with the homoleptic copper complexes, consistent with the functionalization step in eqn (1).

Conclusions

We have demonstrated that the SALSAC approach to the hierarchical assembly of heteroleptic bis(dimine)copper(i) complexes that we have previously established for annealed nanoparticulate TiO_2 surfaces²⁰ can be extended to NPs dispersed in solution. We have presented a general procedure for the activation of commercial TiO_2 NPs by initial treatment with aqueous HNO_3 . After dispersion in water, the activated NPs were functionalized with anchoring ligands **1–4** by heating under microwave conditions, and the functionalized NPs were investigated using FT-IR, TGA, and ^1H NMR spectroscopy. Ligands **1–3** contain phosphonic acid anchoring groups while **4** has two carboxylic acid anchors; ligands **1, 2** and **4** contain 6,6'- Me_2bpy and **3** contains tpy metal binding domains. NPs functionalized with **1, 2** and **4** react with $[\text{Cu}(\text{MeCN})_4][\text{PF}_6]$ and those with **3** react with $\text{FeCl}_2 \cdot 4\text{H}_2\text{O}$; metal binding has been investigated using solid-state absorption spectroscopy and SEM.

By reacting the activated NPs with mixtures of ligands, competitive binding of ligands to TiO_2 has been investigated. For the phosphonic acids, the binding orders are $3 > 1 > 2$ which can be rationalized in terms of relative pK_a values (phosphonic acid and $[\text{HMe}_2\text{bpy}]^+$ or $[\text{Htpy}]^+$) and the number of anchoring groups in the ligands. Competition experiments between **1** and **4** confirmed preferential binding of phosphonic over carboxylic acid anchors.

The final step in the SALSAC strategy is ligand exchange between ligand-functionalized NPs and homoleptic metal complexes to yield TiO_2 NPs functionalized with heteroleptic complexes. We have demonstrated that this is successful for NPs functionalized with **1** reacted with three different $[\text{Cu}(\text{L}_{\text{ancillary}})_2][\text{PF}_6]$ complexes and for NPs functionalized with **3** reacted with $[\text{Fe}(8)_2][\text{PF}_6]_2$. This approach provides a versatile hierarchical approach to the formation of metal complex-functionalized NPs, and we are currently employing the SALSAC strategy in catalysis and sensing applications.

Conflicts of interest

There are no conflicts to declare.

Acknowledgements

We are grateful to the Swiss National Science Foundation (grant number 200020_182000) and the University of Basel for financial support. DOSY spectroscopy was performed by PD Dr D. Häussinger. TEM and SEM images were measured with the assistance of Susanne Erpel and Evi Bieler, respectively, at the



Nano Imaging Lab, University of Basel and we also thank Dr Markus Dürrenberger. Ligands **3** and **6** were prepared by Alexandra Wiesler and Fabian Brunner (University of Basel), respectively. We also thank Mariia Karpacheva (University of Basel) for supplying $[\text{Fe}(\text{8})_2][\text{PF}_6]_2$.

References

- 1 Z. Ren, Y. Guo, C.-H. Liu and P.-X. Gao, *Front. Chem.*, 2013, **1**, 1.
- 2 *Modern Inorganic Synthetic Chemistry*, ed. R. Xu and Y. Xu, Elsevier, Amsterdam, 2nd edn, 2017.
- 3 *Hierarchical Nanostructures for Energy Devices*, ed. S. H. Ko and C. P. Grigoropoulos, RSC Nanoscience & Nanotechnology, No. 35, RSC, Cambridge, 2015.
- 4 S. Whitelam, *Adv. Mater.*, 2015, **27**, 5720.
- 5 S. Casalini, C. A. Bortolotti, F. Leonardi and F. Biscarini, *Chem. Soc. Rev.*, 2017, **46**, 40.
- 6 A. Ulman, *Chem. Rev.*, 1996, **96**, 1533.
- 7 J. J. Gooding, F. Mearns, W. Yang and J. Liu, *Electroanalysis*, 2003, **15**, 81.
- 8 A. Iyer and K. Paul, *IET Nanobiotechnol.*, 2015, **9**, 122.
- 9 E. Mattia and S. Otto, *Nat. Nanotechnol.*, 2015, **10**, 111.
- 10 F. Tao, *Pure Appl. Chem.*, 2008, **80**, 45.
- 11 S. De Feyter and F. C. De Schryver, *J. Phys. Chem. B*, 2005, **109**, 4290.
- 12 A. Kumar, K. Banerjee and P. Liljeroth, *Nanotechnology*, 2017, **28**, 082001.
- 13 D. N. Reinhoudt, *Perspectives in Supramolecular Chemistry*, Wiley, Chichester, 2008, vol. 20.
- 14 S. Stepanow, N. Lin, J. V. Barth and K. Kern, *J. Phys. Chem. B*, 2006, **110**, 23472.
- 15 A. E. Danks, S. R. Hill and Z. Schnepf, *Mater. Horiz.*, 2016, **3**, 91.
- 16 G. M. Whitesides, E. Ostuni, S. Takayama, X. Jiang and D. E. Ingber, *Annu. Rev. Biomed. Eng.*, 2001, **3**, 335.
- 17 R. E. P. Winpenney, *J. Chem. Soc., Dalton Trans.*, 2002, 1.
- 18 E. Schönhof, B. Bozic-Weber, C. J. Martin, E. C. Constable, C. E. Housecroft and J. A. Zampese, *Dyes Pigm.*, 2015, **115**, 154.
- 19 C. E. Housecroft and E. C. Constable, *Chem. Soc. Rev.*, 2015, **44**, 8386.
- 20 F. J. Malzner, C. E. Housecroft and E. C. Constable, *Inorganics*, 2018, **6**, 57.
- 21 *From system complexity to emerging properties*, ed. M. Aziz-Alaoui and C. Bertelle, Springer, Berlin/Heidelberg, 2009.
- 22 F. J. Malzner, A. Prescimone, E. C. Constable, C. E. Housecroft and M. Willgert, *J. Mater. Chem. A*, 2017, **5**, 4671.
- 23 S. Y. Brauchli, F. J. Malzner, E. C. Constable and C. E. Housecroft, *RSC Adv.*, 2014, **4**, 62728.
- 24 C. E. Housecroft, C. G. Palivan, K. Gademann, W. Meier, M. Calame, V. Mikhalevich, X. Zhang, E. Piel, M. Szponarski, A. Wiesler, A. Lanzilotto, E. C. Constable, A. Fanget and R. L. Stoop, *Chimia*, 2016, **70**, 402.
- 25 For an overview, see: A. Winter, S. Hoepfner, G. R. Newkome and U. S. Schubert, *Adv. Mater.*, 2011, **23**, 3484.
- 26 See for example: W. R. McNamara, R. C. Snoeberger, G. Li, J. M. Schleicher, C. W. Cady, M. Poyatos, C. A. Schmuttenmaer, R. H. Crabtree, G. W. Brudvig and V. S. Batista, *J. Am. Chem. Soc.*, 2008, **130**, 14329.
- 27 S. P. Hill, T. Banerjee, T. Dilbeck and K. Hanson, *J. Phys. Chem. Lett.*, 2015, **6**, 4510.
- 28 See for example: S. Takahashi, S. Hotta, A. Watanabe, N. Idota, K. Matsukawa and Y. Sugahara, *ACS Appl. Mater. Interfaces*, 2017, **9**, 1907; J. Sun, E. J. Petersen, S. S. Watson, C. M. Sims, A. Kassman, S. Frukhtbeyn, D. Skrtic, M. T. Ok, D. S. Jacobs, V. Reipa, Q. Ye and B. C. Nelson, *Acta Biomater.*, 2017, **53**, 585; R. Bhandary, J. G. Alauzun, P. Hesemann, A. Stocco, M. In and P. H. Mutin, *Soft Matter*, 2017, **13**, 8023; J. Kirschner, J. Will, T. J. Rejek, L. Portilla, M. Berlinghof, P. Schweizer, E. Spiecker, H.-G. Steinrück, T. Unruh and M. Halik, *Adv. Mater. Interfaces*, 2017, **4**, 1700230; L. Zeininger, L. M. S. Stiegler, L. Portilla, M. Halik and A. Hirsch, *ChemistryOpen*, 2018, **7**, 282 and references therein.
- 29 See for example: M. Nilsing, S. Lunell, P. Persson and L. Ojamäe, *Surf. Sci.*, 2005, **582**, 49; C. Queffelec, M. Petit, P. Janvier, D. A. Knight and B. Bujoli, *Chem. Rev.*, 2012, **112**, 3777.
- 30 V. Spampinato, N. Tuccitto, S. Quici, V. Calabrese, G. Marletta, A. Torrisi and A. Licciardello, *Langmuir*, 2010, **26**, 8400.
- 31 A. J. Stephens, F. J. Malzner, E. C. Constable and C. E. Housecroft, *Sustainable Energy Fuels*, 2018, **2**, 786.
- 32 R. Calzada, C. M. Thompson, D. E. Westmoreland, K. Edme and E. A. Weiss, *Chem. Mater.*, 2016, **28**, 6716.
- 33 J. De Roo, K. De Keukeleere, Z. Hens and I. Van Driessche, *Dalton Trans.*, 2016, **45**, 13277.
- 34 J. De Roo, Z. Zhou, J. Wang, L. Deblock, A. J. Crosby, J. S. Owen and S. S. Nonnenmann, *Chem. Mater.*, 2018, **30**, 8034.
- 35 L. Du, W. Wang, C. Zhang, Z. Jin, G. Palui and H. Mattoussi, *Chem. Mater.*, 2018, **30**, 7269.
- 36 C. Goldmann, F. Ribot, L. F. Peiretti, P. Quaino, F. Tielens, C. Sanchez, C. Chanéac and D. Portehault, *Small*, 2017, **13**, 1604028.
- 37 V. Grigel, L. K. Sagar, K. De Nolf, Q. Zhao, A. Vantomme, J. De Roo, I. Infante and Z. Hens, *Chem. Mater.*, 2018, **30**, 7637.
- 38 M. L. Kessler, H. E. Starr, R. R. Knauf, K. J. Rountree and J. L. Dempsey, *Phys. Chem. Chem. Phys.*, 2018, **20**, 23649.
- 39 R. R. Knauf, J. C. Lennox and J. L. Dempsey, *Chem. Mater.*, 2016, **28**, 4762.
- 40 M. La Rosa, T. Avellini, C. Lincheneau, S. Silvi, I. A. Wright, E. C. Constable and A. Credi, *Eur. J. Inorg. Chem.*, 2017, **2017**, 5143.
- 41 A. Ritchhart and B. M. Cossairt, *Inorg. Chem.*, 2019, **58**, 2840.
- 42 G. J. Kubas, *Inorg. Synth.*, 1979, **19**, 90.
- 43 A. Hernández Redondo, Ph.D. thesis, University of Basel, 2009, http://edoc.unibas.ch/diss/DissB_8757.
- 44 B. Bozic-Weber, S. Y. Brauchli, E. C. Constable, S. O. Fürer, C. E. Housecroft, F. J. Malzner, I. A. Wright and J. A. Zampese, *Dalton Trans.*, 2013, **42**, 12293.



- 45 F. Brunner, S. Graber, Y. Baumgartner, D. Häussinger, A. Prescimone, E. C. Constable and C. E. Housecroft, *Dalton Trans.*, 2017, **46**, 6379.
- 46 J. Wang and G. S. Hanan, *Synlett*, 2005, 1251.
- 47 E. C. Constable, J. Lewis, M. C. Liptrot and P. R. Raithby, *Inorg. Chim. Acta*, 1990, **178**, 47.
- 48 <https://www.aerosil.com/sites/lists/RE/DocumentsSI/TI-1243-Titanium-Dioxide-as-Photocatalyst-EN.pdf>, accessed 31 July 2019.
- 49 L. Zhang and J. M. Cole, *ACS Appl. Mater. Interfaces*, 2015, **7**, 3427.
- 50 M. K. Eggleston, D. R. McMillin, K. S. Koenig and A. J. Pallenberg, *Inorg. Chem.*, 1997, **36**, 172.
- 51 N. A. Gothard, M. W. Mara, J. Huang, J. M. Szarko, B. Rolczynski, J. V. Lockard and L. X. Chen, *J. Phys. Chem. A*, 2012, **116**, 1984.
- 52 Y. M. Klein, M. Willgert, A. Prescimone, E. C. Constable and C. E. Housecroft, *Dalton Trans.*, 2016, **45**, 4659.
- 53 S. P. Pujari, L. Scheres, A. T. M. Marcelis and H. Zuilhof, *Angew. Chem., Int. Ed.*, 2014, **53**, 6322.
- 54 B. Kim, S. W. Park, J.-Y. Kim, K. Yoo, J. A. Lee, M.-W. Lee, D.-K. Lee, J. Y. Kim, B. S. Kim, H. Kim, S. Han, H. J. Son and M. J. Ko, *ACS Appl. Mater. Interfaces*, 2013, **5**, 5201.
- 55 See for example: A. Estrada-Monje, R. Zitzumbo-Guzmán, J. A. Bañuelos-Díaz and E. A. Zaragoza-Contreras, *Mater. Chem. Phys.*, 2019, **235**, 121760.
- 56 B. Bozic-Weber, E. C. Constable, C. E. Housecroft, P. Kopecky, M. Neuburger and J. A. Zampese, *Dalton Trans.*, 2011, **40**, 12584.
- 57 B. Bozic-Weber, V. Chaurin, E. C. Constable, C. E. Housecroft, M. Meuwly, M. Neuburger, J. A. Rudd, E. Schönhofer and L. Siegfried, *Dalton Trans.*, 2012, **41**, 14157.
- 58 P. Péchy, F. P. Rotzinger, M. K. Nazeeruddin, O. Kohle, S. M. Zakeeruddin, R. Humphry-Baker and M. Grätzel, *J. Chem. Soc., Chem. Commun.*, 1995, 65.
- 59 A. Moissette, Y. Batonneau and C. Brémard, *J. Am. Chem. Soc.*, 2001, **123**, 12325.
- 60 *Metal Phosphonate Chemistry: From Synthesis to Applications*, ed. A. Clearfield and K. Demadis, RSC Publishing, 2011, ch. 5, p. 166.
- 61 G. Clauti, G. Zassinovich and G. Mestroni, *Inorg. Chim. Acta*, 1986, **112**, 103.
- 62 G. D. Stevens and R. A. Holwerda, *Inorg. Chem.*, 1984, **23**, 2777.
- 63 See for example: A. D. Burrows, R. W. Harrington and M. F. Mahon, *Acta Crystallogr., Sect. C: Cryst. Struct. Commun.*, 1999, **55**, 1921; W. S. Wu, *Acta Crystallogr., Sect. E: Struct. Rep. Online*, 2011, **67**, o2070; E. C. Constable, C. E. Housecroft, M. Neuburger, P. Rösel, G. E. Schneider, J. A. Zampese, F. Monti, N. Armaroli, R. D. Costa and E. Orti, *Inorg. Chem.*, 2013, **52**, 885.
- 64 E. Farkas, É. A. Enyedy, G. Micera and E. Garribba, *Polyhedron*, 2000, **19**, 1727.
- 65 M. K. Nazeeruddin, S. M. Zakeeruddin, R. Humphry-Baker, T. A. Kaden and M. Grätzel, *Inorg. Chem.*, 2000, **39**, 4542.
- 66 See for example: F. J. Malzner, S. Y. Brauchli, E. C. Constable, C. E. Housecroft and M. Neuburger, *RSC Adv.*, 2014, **4**, 48712; A. Büttner, S. Y. Brauchli, E. C. Constable and C. E. Housecroft, *Inorganics*, 2018, **6**, 40.
- 67 A. K. Ichinaga, J. P. Kirchhoff, D. R. McMillin, C. O. Dietrich-Buchecker, P. A. Marnot and J. P. Sauvage, *Inorg. Chem.*, 1987, **26**, 4290.
- 68 M. T. Miller, P. K. Gantzel and T. B. Karpishin, *Inorg. Chem.*, 1998, **37**, 2285.

